Metallicity in crystals of the quasi-one-dimensional rhodate $Ba_{1.2}Rh_8O_{16}$

W. Kobayashi,* S. Hébert, O. Pérez, D. Pelloquin,† and A. Maignan
Laboratoire CRISMAT, ENSICAEN, UMR 6508 CNRS, 6 boulevard Maréchal Juin, 14050 CAEN Cedex 4, France
(Received 18 July 2008; revised manuscript received 28 November 2008; published 27 February 2009)

Single crystals of the quasi-one-dimensional oxide $Ba_{1.2}Rh_8O_{16}$ have been grown, crystallizing in the hollandite-type structure. These crystals show a metalliclike resistivity, with $\rho \sim 0.56$ mΩ cm at 300 K. The thermopower is positive, with $S \sim 20$ μV/K at 300 K. A peak in the thermopower is observed at $T \sim 100$ K, leading to a maximum power factor equal to 30 μW/cm K^2 at 75 K, which is comparable to the one of the Na_xCoO_2 single crystal at 300 K. The metalliclike character of this compound is interpreted by considering the large rhodium oxidation state ($\sim$3.7) responsible for the large charge-carrier concentration ($\sim 10^{22}$ cm^{-3}) estimated by Hall measurements. The origin of the peak in the $S(T)$ at low T is also discussed.

DOI: 10.1103/PhysRevB.79.085207 PACS number(s): 72.15.Jf, 71.10.Pm

I. INTRODUCTION

In strongly correlated electron systems, thermoelectric oxides are an attractive topic. After the discovery of large thermopower in Na_xCoO_2,[1] transition-metal oxides have been extensively studied and several two-dimensional (2D) materials with CdI_2-type CoO_2 layers were found to be good thermoelectrics.[2,3] Apart from cobaltates, interestingly, rhodium oxides such as Sr_xRhO_2,[4] $[Bi_2Ba_2O_4][RhO_2]_{1.8}$,[5,6] $Cu_{1-x}Ag_xRh_{1-y}Mg_yO_2$,[7] and $Bi_{0.78}Sr_{0.4}RhO_{3+\delta}$ (Ref. 8) all containing CdI_2-type RhO_2 layers also show high thermoelectric power. According to the extended Heikes formula proposed by Koshibae *et al.*,[9] spin and orbital degeneracies on mixed-valence state of low-spin Co^{3+} ($3d^6$) and Co^{4+} ($3d^5$) play an important role for the large thermopower. The isoelectronic structures of $4d^6/4d^5$ Rh^{3+}/Rh^{4+} might explain the similarity of the physical properties for cobaltates and rhodates.[6]

One-dimensional (1D) material is very interesting from both physical and technological points of view. Superconductivity, Tomonaga-Luttinger liquid,[10] charge-density wave (CDW), and spin-density wave (SDW) (Ref. 11) are observed in 1D materials such as carbon nanotube,[12] oxides such as $K_{0.3}MoO_3$,[11] and $Na_{0.33}V_2O_5$,[13] and also in organic conductors.[14] On the other hand, only few studies for thermoelectric properties have been devoted to the 1D transition-metal oxides $Ca_3MM'O_6$.[15] Because resistivity is generally high in the 1D system due to several instabilities such as CDW, SDW, and Anderson localization, though high thermopower S values are reported, thermoelectric figure of merit defined by $Z=S^2/\rho\kappa$, with ρ the electrical resistivity and κ the thermal conductivity, is still too small.

Quasi-one-dimensional (quasi-1D) hollandites are denoted by $A_xB_8O_{16}$ (A=K, Li, Sr, Ba, and Bi; B=Ti, V, Mn, Ru, and Rh). This crystal structure consists of ribbons built of double chains of edge-shared BO_6 octahedra, similar to the ones observed in CdI_2 type structure [e.g., Sr_xRhO_2 (Ref. 4)]. The corner shared ribbons form a tunnel BO_2 framework which contain A ions (see Fig. 1). The mixed-valence state between B^{3+} and B^{4+} is realized by the content x of the A cation. According to the width of the tunnel and the ionic radius of the A ion, tetragonal or monoclinic symmetries are realized. While the hollandites with B=Mo,[16,17] Ti, V [for V valency smaller than 3.4 in $Bi_xV_8O_{16}$ (Ref. 18)], and Mn (Ref. 19) show insulating behavior, Ru hollandites show good metallicity with $\rho_{300\ K} \sim 1$ mΩ cm,[20,21] for a nominal Ru valency of 3.67. In addition, polycrystalline hollandite rhodate, $(Ba,Bi)_{1.54}Rh_8O_{16}$ with formal Rh valency of $\sim$3.15, also shows rather low resistivity of 14 mΩ cm at 300 K,[22] though the temperature dependence is semiconductinglike ($d\rho/dT<0$). Thus, according to the expected low resistivity and large thermopower of rhodates with Rh^{3+}/Rh^{4+}, we focused our attention on the quasi-1D-hollandite $Ba_xRh_8O_{16}$ (see Fig. 1). In this paper, we report on the transport properties of $Ba_{1.2}Rh_8O_{16}$ crystals which exhibit a hollandite-type structure. A clear metal-like behavior is observed with resistivity value comparable to isostructural $Ba_{4/3}Ru_8O_{16}$ ruthenates.[20]

II. EXPERIMENTAL

Needlelike single-crystal samples of $Ba_{1.2}Rh_8O_{16}$ were synthesized by a flux method. First, polycrystalline sample of $Bi_{1.8}Ba_2Rh_{1.9}O_y$ was prepared by a solid-state reaction in air according to the method reported by Okada.[5] Then Bi_2O_3 was added as a flux in a weight ratio of $Bi_{1.8}Ba_2Rh_{1.9}O_y:Bi_2O_3=1:5$ so that the total weight should be 6 g. After heating at 1100 °C for 5 h, the mixture was then slowly cooled down to 900 °C at a rate of −5 °C/h in

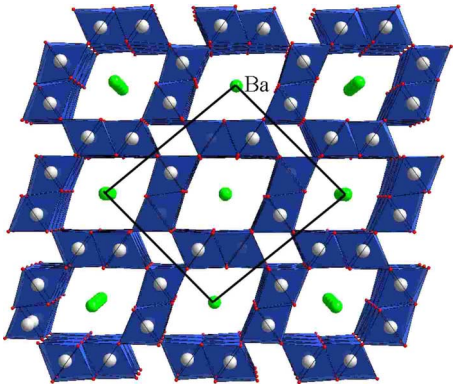

FIG. 1. (Color online) Drawing of the hollandite structure oriented along the [010] direction.

an alumina crucible. Needlelike black shiny crystals with a typical dimension of $1\times0.05\times0.05$ mm^3 were extracted from the melt.

Structural analyses in diffraction mode have been performed with a JEOL 2010Cx transmission electron microscopes (TEM) operating at 200 kV and equipped with an Inca OXFORD EDX analyzer. The high-resolution electron microscopy (HREM) images have been recorded with a JEOL 2010 FEG transmission electron microscopes operating also to 200 kV (Cs=1 mm).

XRD investigation of a high quality single crystal was performed using Mo $K\alpha$ radiations on a Kappa charge-coupled device (CCD) (Bruker Nonius) diffractometer equipped with a CCD detector. Frames were collected through a Φ- and Ω-scans strategy. The diffracted intensities were collected up to $\theta=42°$. Plots of reciprocal-lattice planes assembled from these series of experimental frames are sufficiently accurate to obtain an overall view of the reciprocal space. The EVALCCD software was used to extract reflections from the collected frames. Data were corrected from absorption using JANA2006 program[23] within the analytical option based on the crystal morphology.

All measurements were performed by using a Physical Properties Measurements System (PPMS Quantum Design). The resistivity along the needle direction was measured by a four-probe method from 2.5 to 400 K. To attach four gold wires with diameter of 20 μm to a crystal, silver paste (DuPont 6838) was used. The crystal was heated at 673 K for 10 min to harden the paste and obtain good contacts. The magnetoresistance was measured from 2.5 to 100 K under 0–7 T. The thermoelectric power was measured by a steady-state technique from 5 to 320 K in the PPMS. First, two gold wires were glued to both ends of a needlelike crystal using the silver paste (DuPont 6838). Then, the crystal with the wires were bridged between two heat sinks made of copper plates, and it was glued to the heat sinks using another silver paste (DuPont 4922). To obtain better electrical and thermal contacts, the two gold wires were also glued to the heat sinks. Since the crystal was too small to fix the thermocouple, it was fixed to the heat sink using the silver paste (DuPont 4922). A small temperature gradient of about 1 K was generated by a small resistive heater. The sample voltage was detected through chromel wires. The thermopower of the wire was carefully subtracted. The Hall-coefficient measurement along the c axis was performed by applying −7 to 7 T. As shown in Fig. 4, four terminals made by gold wire and silver paste (DuPont 6838) are put on the crystal with a thickness of 40 μm. Typical signal of ΔV_{xy} was 5 μV and a clear linear dependence of $\Delta R_{xy}(H)$ was obtained. A small extra contribution to $\Delta R_{xy}(H)$ due to misalignments of the terminals was carefully subtracted by using the equation of $[\Delta R_{xy}(H)-\Delta R_{xy}(-H)]/2$.

III. STRUCTURAL INVESTIGATIONS

Several "needlelike" crystals have been studied by TEM. The analysis of these selected crystals in diffraction mode reveals a monoclinic structure with a I-type symmetry and the following cell parameters:

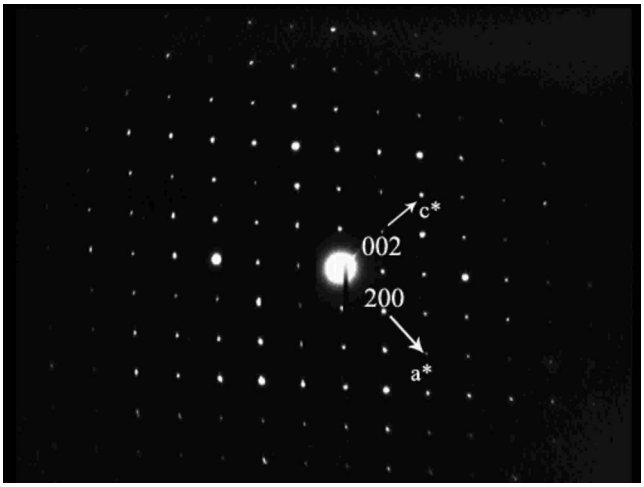

(a)

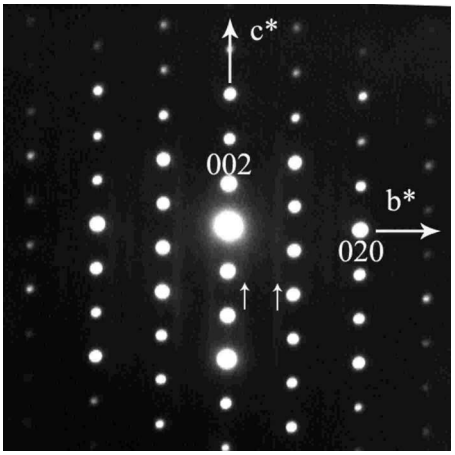

(b)

FIG. 2. Experimental electron-diffraction patterns oriented along the (a) [010] and (b) [100] directions. The spots are indexed in the monoclinic $I2/m$ space group.

$$a\approx 10.4\ \text{Å},\quad b\approx 3\ \text{Å},\quad c\approx 9.4\ \text{Å}$$

$$\text{and}\quad \beta\approx 95°\ \text{(black cell in Fig. 1)}.$$

This work in agreement with the previous results reported by Klimczuk *et al.*[22] is summarized by the [010] and [001] oriented electron-diffraction (ED) patterns (Fig. 2) in which all the main spots can be indexed in the $I12m$ space group. Additionally, the coupled energy spectroscopy analyses (EDS) yield an average cationic composition "$Ba_{1.2}Rh_8$," demonstrating that bismuth was not incorporated in the crystals in contrast to the polycrystalline compound $Ba_{1.2}Bi_{0.33}Rh_8O_{16}$.[22] This indicates the existence of a large A cation deficiency in the $A_xB_8O_{16}$ formula, at least the largest in the case of the barium based rhodate $Ba_xRh_8O_{16}$. As previously observed in the $(Ba,Bi)_{1.54}Rh_8O_{16}$ hollandite structure,[22] satellite spots along b^* axis or diffuse lines parallel to [h0k] direction are systematically observed [white arrows in Fig. 2(b)]. This point is confirmed by the analysis of the x-ray single-crystal diffraction patterns that exhibit also two sets of reflections. The intense ones are character-

TABLE I. Positional parameters.

Atoms	x	y	z	u_{iso}
Rh(1)	0.16124(8)	0.5	0.34200(8)	0.0035(2)
Rh(2)	0.14104(7)	0	0.67150(8)	0.0032(2)
Ba(1)	0	0	0	0.184(4)
O(1)	0.3369	0	0.6863	0.003902
O(2)	0.0437	0	0.2931	0.004666
O(3)	0.2904	0	0.3626	0.004661
O(4)	0.3704	0	0.9595	0.005462

istic of a monoclinic cell with the following refined parameters:

$$a = 10.4461(4)\ \text{Å}, \quad b = 3.0514(3)\ \text{Å},$$

$$c = 9.4236(6)\ \text{Å}, \quad \beta = 93.88(4)^\circ,$$

while the weaker ones are in incommensurate position and their indexation requires the introduction of an additional vector: $\mathbf{q}^* = \mathbf{0.231(2)b}^*$. The observed conditions limiting the possible reflections, $hkl: h+k+l=2n$, are consistent with the $I2/m$ space group.

Owing to the existence of the supplementary reflections in incommensurate position, the accurate structure determination requires superspace approach. Like in Ref. 22, these superstructures can be ascribed to the incommensurate preferential occupation of the (Ba,Bi) cations along the tunnels of the Rh_8O_{16}. This investigation will be reported in a paper devoted to a detailed analysis of the ordering of the guest cations in a series of hollandite structure.[24]

An average structure has been solved with Superflip[25] using charge-flipping methods. Then, a classical hollandite Rh_8O_{16} framework is obtained consisting in a corner sharing of four double edge sharing rutile $[Rh_2O_4]_\infty$ chains (Fig. 1). This framework forms square tunnels running along **b**. The barium atoms are located in the tunnels. This model was subsequently introduced in the refinement program JANA2006,[23] all the atomic positions were refined and anisotropic atomic displacement parameters (ADPs) were considered for all the atoms. The refinement parameters are gathered in Tables I and II. The large ADP observed for Ba(1) along **b** is related to the incommensurate modulation; it can be attributed to both Ba atomic displacements and vacancies distribution. The refinement led to an agreement factor of ~7.1%.

TABLE II. ADP harmonic parameters (u_{12} and u_{23} are blocked by symmetry).

Atoms	u_{11}	u_{22}	u_{33}	u_{13}
Rh(1)	0.0037(3)	0.0040(4)	0.0030(3)	0.0010(2)
Rh(2)	0.0034(3)	0.0039(4)	0.0025(3)	0.0006(2)
Ba(1)	0.0175(9)	0.519(11)	0.0143(9)	0.0003(7)
O(1)	0.003(3)	0.006(3)	0.002(3)	0.000(2)
O(2)	0.004(3)	0.002(3)	0.008(3)	–0.001(2)
O(3)	0.005(3)	0.007(3)	0.002(3)	0.003(2)
O(4)	0.008(3)	0.007(3)	0.001(3)	0.001(2)

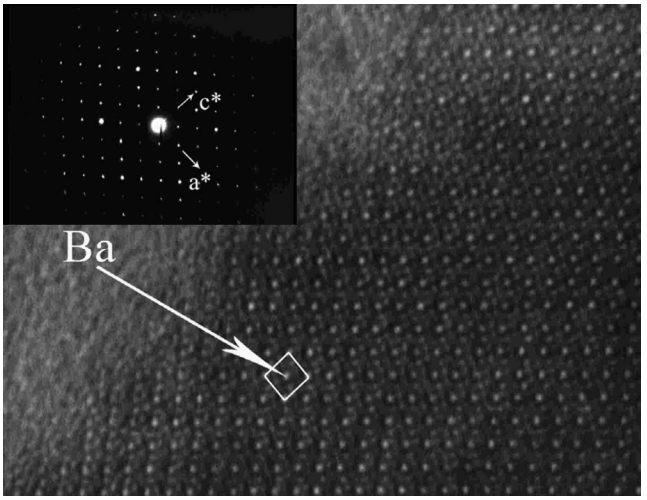

FIG. 3. Experimental [100] oriented HREM image. The hollandite cell is drawn (white line) and the Ba row are identified by the white arrows.

Despite this complex nanostructural features, the hollandite framework of the present $Ba_{1.2}Rh_8O_{16}$ crystals has been checked by HREM technique. This point is illustrated by the [010] oriented image shown in Fig. 3 in which the barium and rhodium atomic rows can be correlated with bright and gray dots, respectively. Such an image contrast is in perfect agreement with the expected hollandite-type structure (Fig. 1) and confirms the structural type for the $Ba_{1.2}Rh_8O_{16}$ crystals.

IV. PHYSICAL PROPERTIES

Figure 4 shows resistivity ρ along the needle direction. At 300 K, the magnitude of resistivity is 0.56 mΩ cm, and the

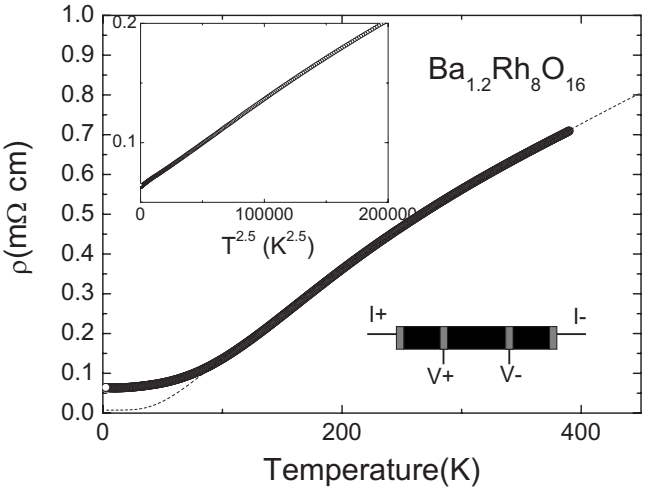

FIG. 4. Resistivity of $Ba_{1.2}Rh_8O_{16}$. The dot line represents the Bloch-Grüneisen fit $\rho^{-1}(T) = \rho_{sat}^{-1} + [\rho(0) + A(T/\theta_D)^5 J_5(T/\theta_D)]^{-1}$. The inset shows resistivity as a function of $T^{2.5}$.

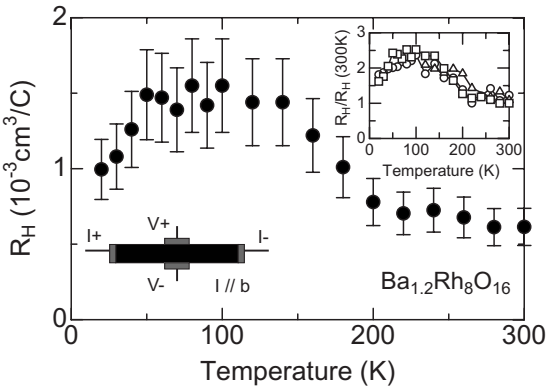

FIG. 5. Hall coefficient R_H of $Ba_{1.2}Rh_8O_{16}$. The inset shows $R_H(T)/R_H$ (300 K) data of three samples.

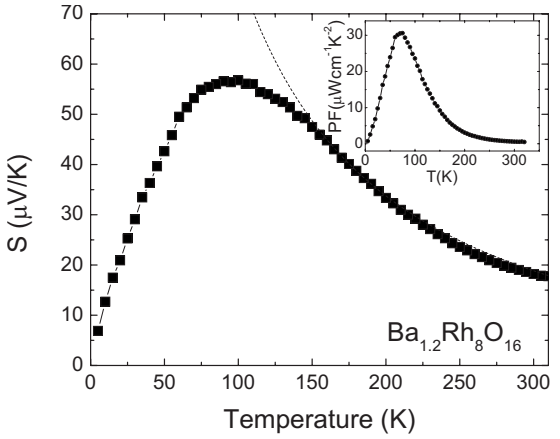

FIG. 6. Thermopower of $Ba_{1.2}Rh_8O_{16}$. The dotted line shows the T^{-1} behavior for $T>100$ K.

value goes down to 65 $\mu\Omega$ cm at 2.5 K. This value at 300 K is comparable with the resistivity of the hollandite ruthenates, $\rho=0.2$ mΩ cm for $BaRu_6O_{12}$ (Ref. 20) and $\rho=0.37$ mΩ cm for $Cs_{0.8}Li_{0.2}Ru_4O_8$ at 300 K.[21] This metallike behavior ($d\rho/dT>0$) in $Ba_{1.2}Rh_8O_{16}$ is observed for the hollandite rhodium oxides. For instance, the polycrystalline $(Ba,Bi)_{1.54}Rh_8O_{16}$ compound shows rather large ρ of 14 mΩ cm at 300 K with semiconducting behavior.[22] Taking into account the smallest occupancy of tunnel sites for the present crystals, "$Ba_{1.2}$" against "$Ba_{1.21}Bi_{0.33}$," a higher oxidation state (v_{Rh}) is calculated from the chemical formula, $v_{Rh}=3.7$ for $Ba_{1.2}Rh_8O_{16}$ ($v_{Rh}=3.57$ for $Ba_{1.2}Bi_{0.33}Rh_8O_{16}$). This could explain the smaller ρ together with metal-like conduction for the former.

In order to compare the charge-carrier concentrations, measurements of the Hall coefficient R_H was made along the needle direction (Fig. 5). At 300 K, the value is 6.14×10^{-4} cm^3/C, which corresponds to high carrier concentration of 1.01×10^{22} cm^{-3}. This carrier concentration is almost the same as 1.7×10^{22} cm^{-3} of the Ru-based hollandite[20] and also near that in Na_xCoO_2.[1] Above 200 K, R_H is almost temperature independent, but below 200 K, the value slightly changes and also a peak is observed at around 100 K.

For $T>100$ K, the temperature dependence of resistivity (Fig. 4) is typical of a classical metal and can be fitted by the Bloch-Grüneisen formula, characteristic of electron-phonon diffusion: $\rho^{-1}(T)=\rho_{sat}^{-1}+[\rho(0)+A(T/\theta_D)^5J_5(T/\theta_D)]^{-1}$.[26] This formula is valid for isotropic materials. Nevertheless, other anisotropic metallic materials also obey this Bloch Grüneisen model such as $Bi_2Sr_{2-x}La_xCuO_{6+\delta}$,[27] CaC_6,[28] or in $YBa_2Cu_4O_8$.[29] The analytical expression for the J_5 function has been calculated as shown in Ref. 30. The fitted curve is presented in Fig. 4, and gives $\theta_D=310$ K [with $\rho(0)=0.0075$ mΩ cm, $A=2.72$ mΩ cm, and $\rho_{sat}=5$ mΩ cm] as fitting parameters. As shown in the inset of Fig. 4, for $T<120$ K, the Bloch-Grüneisen law is not followed and ρ is proportional to $T^{2.5}$. This power is not conventional compared for example to the T^2 behavior due to electron-electron scattering. A similar $T^{2.5}$ power was also observed in quasi-one-dimensional Nb_2Se_3.[31] According to the theory for electrical conduction in quasi-one-dimensional compounds,[32] the origin may be electron-electron-umklapp scattering on the material with quasi-1D band structure which consists of two pairs of planelike Fermi surfaces separated by about half the reciprocal-lattice vector along the chain axis. In this case, the resistivity is proportional to T^n where $2\leq n\leq3$ depending on the relative position of the two pairs of Fermi surfaces. Thus, such a power of the resistivity is typical of quasi-one-dimensionality. Band-structure calculation would be useful to get more details about the origin of this power law.

Figure 6 shows thermopower measured along the needle direction. At 300 K, a rather small value of +20 μV/K is observed. With decreasing temperature, the thermopower increases to reach a maximum value of 60 μV/K at 70 K. The $S(T)$ curve follows at low T a linear dependence $S\sim T$, and above the peak $S\sim1/T$. This peak structure is not expected since a conventional metal should show T-linearlike small $|S|$. Such a peak is also not observed in layered-rhodium oxides with CdI_2-type RhO_2 layers. For the Ru-based hollandite, the same shape of $S(T)$ has been reported, but the thermopower peak value is smaller, with 14 μV/K is observed at 80 K,[21] which is four times smaller than our observation. The inset of Fig. 6 shows power factor PF (PF$=S^2/\rho$), often used to compare the thermoelectric materials in the absence of thermal-conductivity data. At around 100 K, the value is 30 μW/cm K^2, which is near to 50 μW/cm K^2 of Na_xCoO_2 (Ref. 1) and 40 μW/cm K^2 of Bi_2Te_3 at 300 K. As far as we know, the PF of $Ba_{1.2}Rh_8O_{16}$ is the largest among quasi-1D oxides.

Due to the small size of crystals, magnetic-susceptibility measurements could not be performed. To test a possible magnetic origin for the peaks observed in the Seebeck and Hall measurements, isothermal measurements of magnetoresistance were also performed (Fig. 7). Above 10 K, MR is positive and the value is very small, while below 10 K, negative MR is observed. This negative MR corresponds to reentrant resistivity observed below ~10 K. This temperature, much lower than the peak temperature of ~100 K might be a signature of an instability such as CDW, SDW, or other mechanism. Clearly, application of an external magnetic field suppresses the localization. Such a negative magnetoresistance of small magnitude (−2.5% in 7 T at 2.5 K) does not occur in conventional metal.

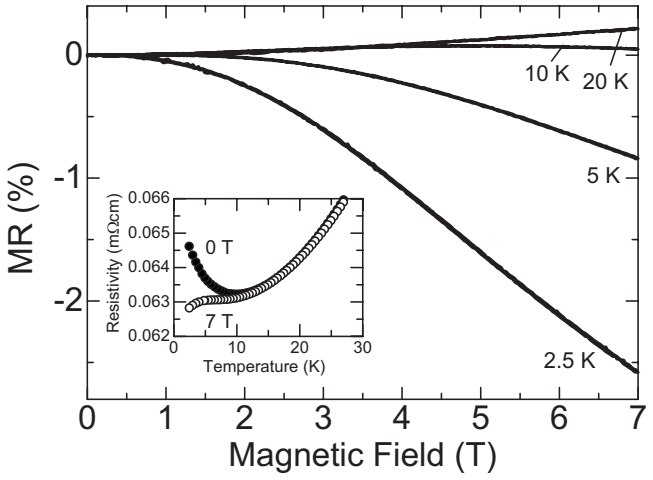

FIG. 7. Magnetoresistance of $Ba_{1.2}Rh_8O_{16}$ below 100 K. The inset shows resistivity under 0 and 7 T below 30 K.

V. DISCUSSION

Only few hollandite oxides are found to be metallic. Single crystals of $Ba_{4/3}Ru_8O_{16}$ (Ref. 20) possess a metallic behavior along the needle direction. Also, a metallic behavior is observed in the polycrystals of KRu_4O_8, $RbRu_4O_8$, or single crystals of $Cs_{0.8}Li_{0.2}Ru_4O_8$.[21] This metallicity could be attributed to the 4*d* orbitals which favor a larger overlap than in the 3*d* case. Nevertheless, metallicity is also reported in the case of 3*d* such as $Bi_xV_8O_{16}$, if $1.60 \leq x \leq 1.71$.[33] The carrier density therefore plays also a crucial role in the metallicity, and the large carrier density of 1.02×10^{22} cm^{-3} in $Ba_{1.2}Rh_8O_{16}$ favors a metallic behavior.

This metallic behavior can be described by classical electron-phonon scattering for $T > 100$ K, as shown by the Bloch-Grüneisen fit of $\rho(T)$. However, $Ba_{1.2}Rh_8O_{16}$ does not exhibit all the characteristics of a metal: $\rho(T)$ does not obey the Bloch-Grüneisen law below 100 K, a decrease in R_H is observed below 100 K, and a peak of $S(T)$ is observed at ~ 100 K, the values of S being large compared to classical metals. In the case of semiconducting hollandites, the thermopower is reported to be negative, and constant from $T \sim 150$ K up to 300 K in $K_{1.5}(H_3O)_xMn_8O_{16}$ (Ref. 19) or in $Rb_{1.5}Mo_8O_{16}$ (Ref. 17) and is explained using the small polaron hopping. On the other hand, in the metallic single crystals of $Cs_{0.8}Li_{0.2}Ru_4O_8$,[21] S also presents a peak of 15 $\mu V/K$ at $T \sim 100$ K, and a linear dependence for $T > 100$ K, with $S = -10$ $\mu V/K$ at 300 K. The curve presented in Fig. 6 also exhibits a peak at $T \sim 100$ K, and a decrease for larger temperature, the values of S being much larger in the case of Rh than in the case of Ru.

The steep peak on the $S(T)$ can originate from several phenomena such as ferromagnetic ordering,[34] phonon drag,[26] minority-carrier excitation (two carrier model),[35] and Kondo effect.[36] The hollandite rhodium oxides usually exhibit paramagnetism as shown in several studies,[22,37] ruling out a possible magnetic origin. Using the two carrier model of thermopower $S = (S_1\sigma_1 + S_2\sigma_2)/(\sigma_1 + \sigma_2)$ [S_i $(i=1,2)$: thermopower of band i, σ_i $(i=1,2)$: conductivity of band i)], minor carrier can also make a peak of thermopower S where $S_2/S_1 \sim -100$, and $\sigma_2/\sigma_1 \ll 1$ as calculated in Fe metal.[35] In this case, the temperature dependence of S would be related to minor-carrier excitation, but this does not explain the peak also observed in the $R_H(T)$ curve.

The classical phonon drag mechanism for thermopower is proportional to the specific heat ($S_{drag} \sim C_V$) which leads to a T^3 dependence of $S(T)$ at low T.[26] In the case of $Cs_{0.8}Li_{0.2}Ru_4O_8$, a T^3 dependence is indeed observed and attributed to the phonon drag. However, in the case of 1D materials, this dependence of specific heat and thus of S_{drag} can be affected, and several models have been developed, for example, for nanotubes.[38] Specific heat measurements, not possible due to the small size of crystals, are required to analyze in more details the $S(T)$ and its relationship with phonon drag. However, it must be emphasized that using the Bloch-Grüneisen fitting of the resistivity, the Debye temperature is close to 300 K. A peak in $S(T)$ is expected at $T \sim \theta_D/5$ in materials where electron-phonon interactions dominate,[39] i.e., at $T \sim 60$ K, not far from the temperature where the peak is observed in Fig. 6. Clearly, the specific heat has to be measured to determine the relationship between S and C_V, and check the validity of this Bloch Grüneisen analysis.

The peak in the $S(T)$ at 75 K induces a maximum power factor $PF = S^2/\rho$ of 30 $\mu W\ cm^{-1}\ K^{-2}$ at 100 K. Even if it is smaller than the peak observed at 75 K in Na_xCoO_2 ($x > 0.85$) of 187 $\mu W\ cm^{-1}\ K^{-2}$ for $Na_{0.88}CoO_2$,[40] it is very close to the value reported at 300 K in $Na_{0.7}CoO_2$.[1] As far as we know, this Rh hollandite presents the largest power factor reported among quasi-one-dimensional oxides.

In the case of metallic perovskites of $SrRhO_3$ and $SrRuO_3$, the thermopower presents similar $S(T)$ dependence, with S positive and $dS/dT > 0$ for $T \leq 300$ K.[41–43] At 300 K, S reaches +35 $\mu V/K$ in $SrRuO_3$,[43] and almost +60 $\mu V/K$ in $SrRhO_3$.[41] It was shown in Ref. 43 that the spin entropy term[44] $S = \frac{-k_B}{|e|}\ln(\frac{2S_n+1}{2S_{n+1}+1})$ associated with the Ru^{3+} $(S_n = 1/2)/Ru^{4+}$ $(S_{n+1} = 1)$, $S_{spin} = +35$ $\mu V/K$, or Ru^{4+} $(S_n = 1)/Ru^{5+}$ $(S_n = 3/2)$, $S_{spin} = +25$ $\mu V/K$, spin states is dominant to explain the value of S at 300 K. The spin entropy term could play a similar role in $SrRhO_3$, and is theoretically larger for Rh than for Ru [$S_{spin} = +60$ $\mu V/K$ for Rh^{3+} $(S_n = 0)/Rh^{4+}$ $(S_{n+1} = \frac{1}{2})$]. This major contribution of the spin entropy term in a metallic system could also explain here why S is larger in this Rh hollandite than in the Ru one, the difference between the two being 25 $\mu V/K$ at 300 K as in metallic perovskites.

VI. CONCLUSIONS

Single crystal of $Ba_{1.2}Rh_8O_{16}$ have been successfully grown. They crystallize in the hollandite structure where the low barium content in tunnels of the Rh_8O_{16} framework is responsible for a large average oxidation state of ~ 3.7 for rhodium species. These crystals exhibit a metallic behavior, classically fitted by a Bloch Grüneisen law for $T > 100$ K. The thermopower is positive and exhibits a peak of 60 $\mu V/K$ at $T \sim 100$ K, with a decrease in S at higher T, with $S \sim T^{-1}$. The origin of the peak might be correlated with a phonon drag mechanism, but specific-heat measurements are required to confirm this hypothesis. Compared to Ru hol-

landites with similar carrier density, the values of Seebeck coefficients are larger in the whole T range. This enhancement of S might be attributed to a spin entropy excess associated to Rh^{3+}/Rh^{4+}. The power factor at 75 K is almost the same as that of Na_xCoO_2 at 300 K, and is the largest among quasi-one-dimensional oxides as far as we know.

ACKNOWLEDGMENTS

The authors thank Alain Pautrat for stimulating discussion and CNRS and ANR OCTE for financial support. This work is in the frame of the FAMENOE European network.

*Present address: Waseda Institute for Advanced Study, Waseda University, Tokyo 169-8050, Japan.

†FAX: 00 33 2 31 95 16 00. denis.pelloquin@ensicaen.fr

[1] I. Terasaki, Y. Sasago, and K. Uchinokura, Phys. Rev. B **56**, R12685 (1997).
[2] R. Funahashi and M. Shikano, Appl. Phys. Lett. **81**, 1459 (2002).
[3] A. C. Masset, C. Michel, A. Maignan, M. Hervieu, O. Toulemonde, F. Studer, B. Raveau, and J. Hejtmanek, Phys. Rev. B **62**, 166 (2000).
[4] Y. Okamoto, M. Nohara, F. Sakai, and H. Takagi, J. Phys. Soc. Jpn. **75**, 023704 (2006).
[5] S. Okada and I. Terasaki, Jpn. J. Appl. Phys. Part 1 **44**, 1834 (2005).
[6] Y. Klein, S. Hébert, D. Pelloquin, V. Hardy, and A. Maignan, Phys. Rev. B **73**, 165121 (2006).
[7] S. Shibasaki, W. Kobayashi, and I. Terasaki, Phys. Rev. B **74**, 235110 (2006).
[8] W. Kobayashi, S. Hébert, D. Pelloquin, O. Perez, and A. Maignan, Phys. Rev. B **76**, 245102 (2007).
[9] W. Koshibae, K. Tsutsui, and S. Maekawa, Phys. Rev. B **62**, 6869 (2000).
[10] S.-I. Tomonaga, Prog. Theor. Phys. **5**, 544 (1951).
[11] G. Grüner, Rev. Mod. Phys. **60**, 1129 (1988).
[12] H. Ishii, H. Kataura, H. Shiozawa, H. Yoshioka, H. Otsubo, Y. Takayama, T. Miyahara, S. Suzuki, Y. Achiba, M. Nakatake, T. Narimura, M. Higashiguchi, K. Shimada, H. Namatame, and M. Taniguchi, Nature (London) **426**, 540 (2003).
[13] T. Yamauchi, Y. Ueda, and N. Mori, Phys. Rev. Lett. **89**, 057002 (2002).
[14] K. Mortensen, Y. Tomkiewicz, T. D. Schultz, and E. M. Engler, Phys. Rev. Lett. **46**, 1234 (1981).
[15] A. Maignan, S. Hébert, C. Martin, and D. Flahaut, Mater. Sci. Eng., B **104**, 121 (2003).
[16] J. Tortelier, W. H. McCarroll, and P. Gougeon, J. Solid State Chem. **136**, 87 (1998).
[17] T. Ozawa, I. Suzuki, and H. Sato, J. Phys. Soc. Jpn. **75**, 014802 (2006).
[18] T. Waki, H. Kato, M. Kato, and K. Yoshimura, J. Phys. Soc. Jpn. **73**, 275 (2004).
[19] H. Sato, T. Enoki, J. I. Yamaura, and N. Yamamoto, Phys. Rev. B **59**, 12836 (1999).
[20] Z. Q. Mao, T. He, M. M. Rosario, K. D. Nelson, D. Okuno, B. Ueland, I. G. Deac, P. Schiffer, Y. Liu, and R. J. Cava, Phys. Rev. Lett. **90**, 186601 (2003).
[21] M. L. Foo, Wei-Li Lee, T. Siegrist, G. Lawes, A. P. Ramirez, N. P. Ong, and R. J. Cava, Mater. Res. Bull. **39**, 1663 (2004).
[22] T. Klimczuk, Wei-Li Lee, H. W. Zandbergen, and R. J. Cava, Mater. Res. Bull. **39**, 1671 (2004).
[23] V. Petricek and M. Dusek, Jana 2006, The crystallographic computing system, Institute of Physics, Praha, Czech Republic.
[24] O. Pérez, P. Roussel, D. Pelloquin, and W. Kobayashi (unpublished).
[25] L. Palatinus and G. Chapuis, Superflip-a computer program for the solution of crystal structures by charge flipping in arbitrary dimensions, J. Appl. Crystallogr. **40**, 786 (2007).
[26] J. M. Ziman, *Electrons and Phonons* (Clarendon, Oxford, 1960).
[27] L. S. Mazov, Phys. Rev. B **70**, 054501 (2004).
[28] E. Jobiliong, H. D. Zhou, J. A. Janik, Y. J. Jo, L. Balicas, J. S. Brooks, and C. R. Wiebe, Phys. Rev. B **76**, 052511 (2007).
[29] B. Bucher, P. Steiner, J. Karpinski, E. Kaldis, and P. Wachter, Phys. Rev. Lett. **70**, 2012 (1993).
[30] B. A. Mamedov and I. M. Askerov, Phys. Lett. A **362**, 324 (2007).
[31] M. H. Rashid and D. J. Sellmyer, Phys. Rev. B **29**, 2359 (1984).
[32] A. Oshiyama, K. Nakao, and H. Kamimura, J. Phys. Soc. Jpn. **45**, 1136 (1976).
[33] H. Kato, T. Waki, M. Kato, K. Yoshimura, and K. Kosuge, J. Phys. Soc. Jpn. **70**, 325 (2001).
[34] N. S. Kini, A. Bentien, S. Ramakrishnan, and C. Geibel, Physica B **359-361**, 1264 (2005).
[35] W. M. MacInnes and K. Schröder, Phys. Rev. B **4**, 4091 (1971).
[36] H. Sato, Y. Abe, H. Okada, T. D. Matsuda, K. Abe, H. Sugawara, and Y. Aoki, Phys. Rev. B **62**, 15125 (2000).
[37] J. R. Plaisier, A. A. C. van Vliet, and D. J. W. IJdo, J. Alloys Compd. **314**, 56 (2001).
[38] V. W. Scarola and G. D. Mahan, Phys. Rev. B **66**, 205405 (2002).
[39] D. K. C. MacDonald, *Thermoelectricity: An Introduction to the Principles* (Wiley, London, 1962).
[40] M. Lee, L. Viciu, L. Li, Y. Wang, M. L. Foo, S. Watauchi, R. A. Pascal, Jr., R. J. Cava, and N. P. Ong, Nature Mater. **5**, 537 (2006).
[41] K. Yamaura, Q. Huang, D. P. Young, Y. Noguchi, and E. Takayama-Muromachi, Phys. Rev. B **66**, 134431 (2002).
[42] K. Yamaura, D. P. Young, and E. Takayama-Muromachi, Phys. Rev. B **69**, 024410 (2004).
[43] Y. Klein, S. Hébert, A. Maignan, S. Kolesnik, T. Maxwell, and B. Dabrowski, Phys. Rev. B **73**, 052412 (2006).
[44] J. P. Doumerc, J. Solid State Chem. **109**, 419 (1994).